Title

Unilateral hippocampal stroke in freely behaving mice reveals sex differences in contralesional spreading depolarization and associated behavior

Authors

Andrew K.J. Boyce[1,2], Yannick Fouad[1,2], Renaud C. Gom[1,2], Cristina Martins-Silva[3], Leonardo Molina[1,2], Tamas Füzesi[1,2], Carina Ens[1,2], Wilten Nicola[1,2], G. Campbell Teskey[1,2], Roger J. Thompson[1,2*]

Affiliations

1. Department of Cell Biology & Anatomy, Cumming School of Medicine, University of Calgary, Calgary, Alberta, T2N 4N1, Canada
2. Hotchkiss Brain Institute, University of Calgary, Calgary, Alberta, T2N 4N1, Canada
3. Department of the Physiological Sciences, Federal University of Espírito Santo, Vitoria, Brazil

*Corresponding author

Corresponding author, email:

Roger Thompson, rjthomps@ucalgary.ca

Abstract

Following stroke, women have worse functional outcomes than men, due in part to more frequent non-focal symptoms, leading to misdiagnosis and lack of treatment. Understanding changes in peri-stroke behavior is critical to improving outcomes. During an ischemic stroke, energy loss in tissue fed by a blocked cerebral vessel induces rapid neuronal death. Next, large depolarizing waves (spreading depolarization, SD) emanate from this ischemic core. While SD in nearby hypoperfused tissue is deleterious, its impact on remote structures is unclear. Behavioural and cognitive symptoms may mirror this biphasic nature of cell death. We present a model for delivering and monitoring focal stroke in awake freely behaving mice, using bilateral fiberoptic cannulas to induce hippocampal stroke (unilateral photothrombosis) and monitor both ipsi- and contralesional neuronal Ca^{2+} dysregulation/dynamics via GCaMP6f photometry. Ipsilesional Ca^{2+} dysregulation, which correlated with lesion size, was indistinguishable between sexes, yet females had larger, more frequent contralesional SD-associated Ca^{2+} waves, with increased acute exploration. Hippocampal stroke generated retrograde and anterograde amnesia, yet anterograde amnesia was absent in mice that had SD-associated Ca^{2+} waves. Fiber photothrombosis with paired photometry offers flexibility to induce and monitor stroke in any brain region in freely behaving mice, allowing interrogation of previously inaccessible stroke biology.

Introduction

Stroke, a localized loss of blood flow in the brain, is second amongst causes of death across the globe, leaving many survivors permanently disabled[1]. Women have worse functional outcomes following stroke than men, which may be based on more frequent misdiagnosis due to the increased likelihood for women to present with non-focal or "atypical" symptoms[2]. The current gold standards in stroke therapy, intravenous tissue plasminogen activator (tPA) and thrombectomy, have relatively short therapeutic windows (up to ~4.5 and 9 hours, respectively)[1], each with diminishing efficacy against disability prevention as time progresses. At present, there is some evidence that tPA is utilized less frequently in women than men[3,4], which is particularly unfortunate as women may benefit more from tPA treatment[5]. This makes an understanding of sex differences in behavior during stroke critical.

An ischemic stroke, responsible for the majority of strokes, occurs in response to a local blockage of blood flow in the brain with neuronal death occurring in two phases: (1) initial necrosis in the ischemic core (< 10 minutes) and (2) subsequent expansion of the core into the hypoperfused neighboring tissue, the penumbra (min to hours). Cognitive and behavioral symptoms of stroke can be focal, linked to the infarcted tissue, or non-focal, a consequence of secondary impacts on neighboring or distant tissue[1]. Within minutes of blood flow disruption, depleted cellular energy substrate adenosine triphosphate (ATP) in the stroke core triggers the failure of energy-dependent homeostatic processes, including maintenance of the resting membrane potential. Large depolarizing transients (spreading depolarizations, SD) then emanate from the core into neighboring gray matter[6,7]. During an SD, calcium influx is enhanced and remains elevated for minutes before returning to baseline[6,8,9]. Spreading depolarizations, first described by Leão[7], severely compromise cellular energy homeostasis, thus they are followed by a relatively brief period of suppressed electrical activity (spreading depression). In the penumbra, neurons have unpredictable outcomes. Here, neurons either undergo a permanent and deadly anoxic depolarization or transient and reversible depolarizations. Although typically limited to ipsilesional tissue, stronger stimuli can elicit symmetric contralateral SD that are weaker, non-coincident and cover less area, than the ipsilesional SD, as seen in Leão's seminal study[7]. Following successive SD, penumbral tissue typically succumbs in the following hours and days, making an understanding of the acute biological and behavioral readouts of stroke particularly important for improving outcomes. While it is generally accepted that SDs in the penumbra worsen outcomes ([10–12] however, see [13]), SDs that reach remote healthy tissue may have a distinct, even beneficial, effect[14]. This benefit could be in the form of pre-conditioning[15] or a generalized increase in plasticity or neurogenic-inducing factors[16–20]. Increased glial proliferation has even been observed in contralesional neurogenic niches[21]. The hippocampus is particularly benefited by the presence of SD, as K^+-evoked SD localized to the cortex induced increased

hippocampal neurogenesis in both rats and mice[17,19] and enhanced object location memory in the weeks following SD[17].

To understand the peri-stroke and long-term behavioral impacts of stroke and SD, we improved upon traditional focal stroke models to allow unilateral stroke induction and recording of neuronal Ca^{2+} dysregulation in ipsilesional and contralesional brain structures of awake and freely behaving (non-anesthetized or head-fixed) mice. To induce unilateral focal stroke in the hippocampus, we utilize photothrombosis, a method pioneered by Rosenblum & El-Sabban[22] and Watson *et al.*[23]. Here, intravascular photo-oxidation of the dye Rose Bengal via implanted optical fiber generated reactive oxygen species which damage the vessel endothelium generating a localized clotting cascade and subsequent ischemia. We record neuronal Ca^{2+} using fibre photometry of the genetically encoded Ca^{2+} biosensor GCaMP6f[24] in hippocampal pyramidal neurons in Thy1GCaMP6f transgenic mice via bilateral fiberoptic cannulas. While ipsilesional Ca^{2+} dysregulation and associated behavior are consistent between females and males, large Ca^{2+} waves that reach the contralesional hippocampus following stroke induction are more frequent and larger in females. These waves are associated with reduced anterograde amnesia following hippocampal stroke, suggesting a protective effect. This model describes a distinct use for fiber photometry, to understand neurodegeneration in real-time, and provides access to previous inaccessible questions in stroke biology.

Results

Anaesthesia alters neuronal Ca^{2+} dynamics during hippocampal stroke in awake freely behaving mice.

We developed a focal stroke model in freely behaving mice for simultaneously recording both ipsilesional and contralesional neuronal Ca^{2+} dysregulation in bilateral hippocampi and analyzing peri-stroke behavior using a combination of fiber photometry and photothrombosis (Fig. 1). Many existing stroke models require invasive surgery to generate ischemia[25]. Inhaled anesthesia (ie. isoflurane) is neuroprotective in models of ischemic stroke in the superficial neocortex, complicating the interpretation of results and masking effects of potential neuroprotectants[26]; however, the effect on anesthesia on ischemic stroke in deeper structures remains unclear. Further, while focal stroke can be triggered in the superficial cortex of awake head-fixed mice[27,28], these approaches (and those elicited under anesthesia) make behavioral evaluation during stroke inaccessible. In our model, chronically implanted optical fibers allow stroke induction and monitoring in the absence of anesthesia or restraint, permitting interrogation of the effects of anesthetic in deeper structures and peri-stroke behavior in awake mice.
We first assessed stroke-evoked neuronal Ca^{2+} dysregulation in the hippocampus of awake versus anesthetized mice; we then used our awake model to evaluate peri-stroke behavior. Neuronal Ca^{2+} dysregulation drives excitotoxic cell death in the acute phase of an ischemic stroke[29]; thus, Thy1-GCaMP6f transgenic mice were

Figure 1. Anaesthesia alters neuronal Ca^{2+} dynamics during hippocampal stroke in awake freely behaving mice.

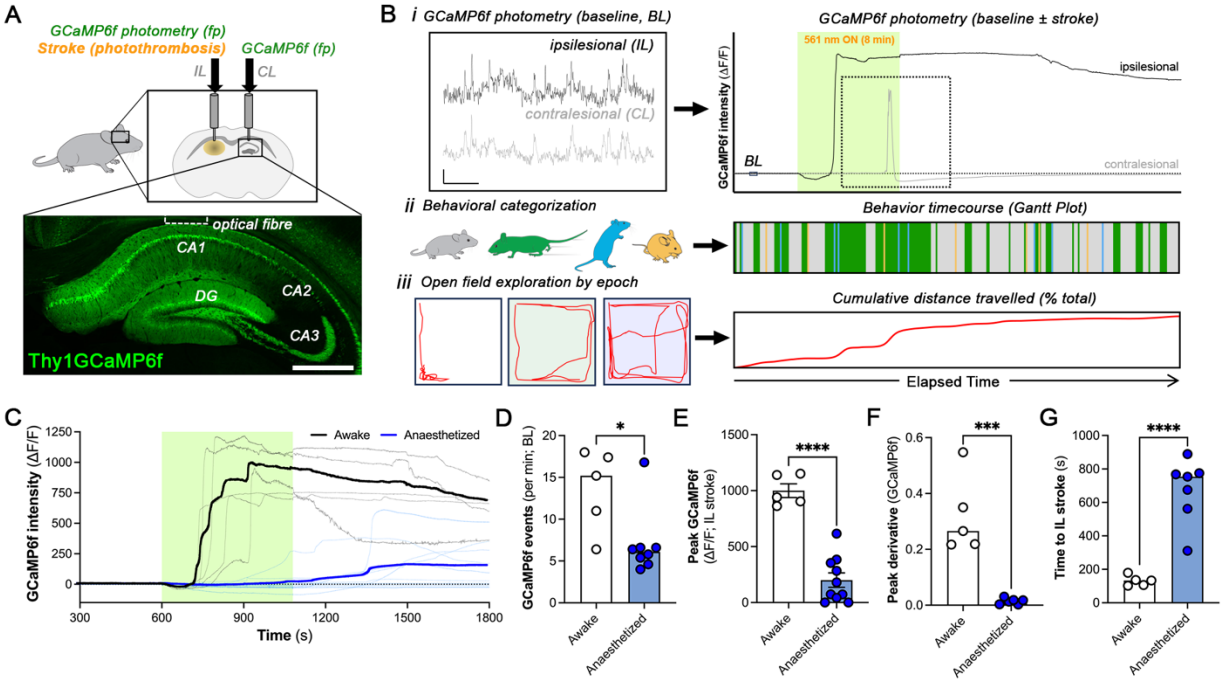

(A) Dual fiberoptic cannulas placed dorsal to bilateral hippocampal CA1 for unilateral hippocampal photothrombotic stroke and bilateral photometry in awake freely behaving Thy1GCaMP6f mice. **(B)** Real-time readouts of (***i***) ipsilesional and contralesional baseline GCaMP6f photometry recordings (scale bar: ΔF/F = 2 arbitrary fluorescence units (arb. units), t = 5 s) and neuronal Ca^{2+} dysregulation in ipsilesional and contralesional hippocampi, paired to (***ii***) categorized behavior and (***iii***) locomotion analyses during 40 min (2400 s) recording in an open field (0.5 m^2). Photothrombotic illumination (561 nm, 6 mW) through fiberoptic cannula dorsal to right CA1 from 600-1080 s (green box). **(C)** Neuronal Ca^{2+} dysregulation (GCaMP6f photometry trace, ΔF/F; mean: thick lines; individual traces: thin lines) induced by fiber photothrombotic stroke in the hippocampus is distinct between awake (black) and anesthetized (blue) mice. Photothrombotic illumination (561 nm, 6 mW, 10-18 min). **(D)** Awake mice have more frequent Ca^{2+} events per min during the baseline epoch than anesthetized mice (awake: 13.6 ± 2.2, n = 5; anesthetized: 7.0 ± 1.4, n = 8; unpaired t-test, *$p < 0.05$). **(E)** Awake mice have larger neuronal Ca^{2+} dysregulation (peak GCaMP6f intensity, ΔF/F) following hippocampal stroke (awake: 999.7 arb. units ± 61.0, n = 5; anesthetized: 200.5 arb. units ± 64.1, n = 8; unpaired t-test, ***$p < 0.001$). ***(F)*** Slope of neuronal Ca^{2+} dysregulation (peak derivative of GCaMP6f) is larger in awake mice (awake: 0.32 ± 0.06, n = 5; anesthetized: 0.04 ± 0.004, n = 6; unpaired t-test, ***$p < 0.001$). **(G)** Onset of neuronal Ca^{2+} dysregulation ($t_{peak\ derivative}$, GCaMP6f) is more rapid in awake mice following onset of photothrombotic illumination (awake: 131.4 s ± 13.8, n = 6; anesthetized: 676.2 s ± 71.7, n = 7; unpaired t-test, ****$p < 0.001$).

used to study neuronal Ca^{2+} dysregulation in the hippocampus in our study. Here, an optical fiber was implanted dorsal to both hippocampi (~ 100 μm dorsal to CA1, Fig. 1a) in Thy1-GCaMP6f mice (> 7 days pre-stroke) to allow photothrombosis and GCaMP6f excitation and emission recording. After recovery and handling, mice were injected (intra-peritoneal, i.p.) with Rose Bengal (1% RB, 0.1 mg/kg) or vehicle (PBS) and either

put under isoflurane anesthetic (5% induction, 1% maintenance) or placed into an open field where CA1 pyramidal neuron GCaMP6f fluorescence (via fiber photometry) and behavior (via overhead camera) were simultaneously recorded (Fig. 1b). Following a 10-min baseline, laser illumination (8 min, 6 mW) through one optical fiber initiated unilateral photo-oxidation of RB, initiating the ischemic cascade (Fig. 1c). To understand differences in basal neuronal activity, neuronal GCaMP6f events were identified over a 10-min baseline recording as an increase in signal > 4 standard deviations above the mean, separated by at least 0.5 s from another peak. Here, awake mice had GCaMP6f events of similar amplitude relative to anesthetized mice ($\Delta F/F \approx 5$ arb. units), however these events occurred at an increased frequency in awake conditions (Fig. 1d). Photothrombosis elicited a large and sustained increase in GCaMP6f intensity (up to ≈ 500-fold of baseline). As in other stroke models, isoflurane anesthesia was protective against focal ischemic stroke[26]. Anesthetized mice had smaller and slower neuronal GCaMP6f dysregulation relative to awake mice under identical photothrombotic illumination (Peak GCaMP6f, Fig. 1e-f). We identified stroke onset as the time when GCaMP6f intensity reaches its maximum rate of change (peak derivative). Here, the onset of stroke was slower under anesthesia (Fig. 1g). Not only does our model allow the examination of peri-stroke behavior, but it also avoids the impact of anesthesia on stroke evolution.

Ipsilesional neuronal Ca^{2+} dysregulation during hippocampal stroke correlates with lesion severity and increased exploration without sex differences.

Neuronal Ca^{2+} dysregulation was evaluated in both ipsilesional and contralesional hippocampi using bilateral fiberoptic cannulas (Fig 2a). In the ipsilesional hemisphere, photothrombosis triggered significant neuronal Ca^{2+} dysregulation, which was absent in shams (vehicle; Fig. 2b). Ipsilesional Ca^{2+} dysregulation was indistinguishable between sexes (Peak GCaMP6f, Fig.2bc). During stroke, no sex differences were observed in the time to the onset of Ca^{2+} dysregulation (time to IL stroke, Fig. 2d) or the maximum rate of change in GCaMP6f fluorescence (peak derivative, Fig. 2e). Neuronal Ca^{2+} dysregulation scaled with illumination time (1.5 – 8 min; 6 mW) and laser power (4 – 6 mW; 1.5 min; Extended Data Fig. 1).
Lesions were assessed using triphenyl tetrazolium chloride (TTC), a live-dead stain relying on functional mitochondria to generate a red product in viable tissue (opaque in infarcted tissue, 48 h post stroke) and immunohistochemistry (7 days post stroke). Stroke lesions (TTC-negative) localized to the ipsilesional hippocampus were indistinguishable between sexes (Fig. 2f). Stroke decreased neuronal GCaMP6f intensity in the ipsilesional hippocampus one week after illumination, indicating neuronal cell loss (Extended Data Fig. 2). While microglial and astrocyte reactivity markers were present surrounding the stroke core, no sex differences were observed (Extended Data Fig. 2). Lesions were smaller in anesthetized mice (Extended Data Fig. 3) and were reduced with decreased laser power/illumination duration in awake mice (Extended

Figure 2. Ipsilesional neuronal Ca^{2+} dysregulation during hippocampal stroke correlates with lesion severity and increased exploration without sex differences.

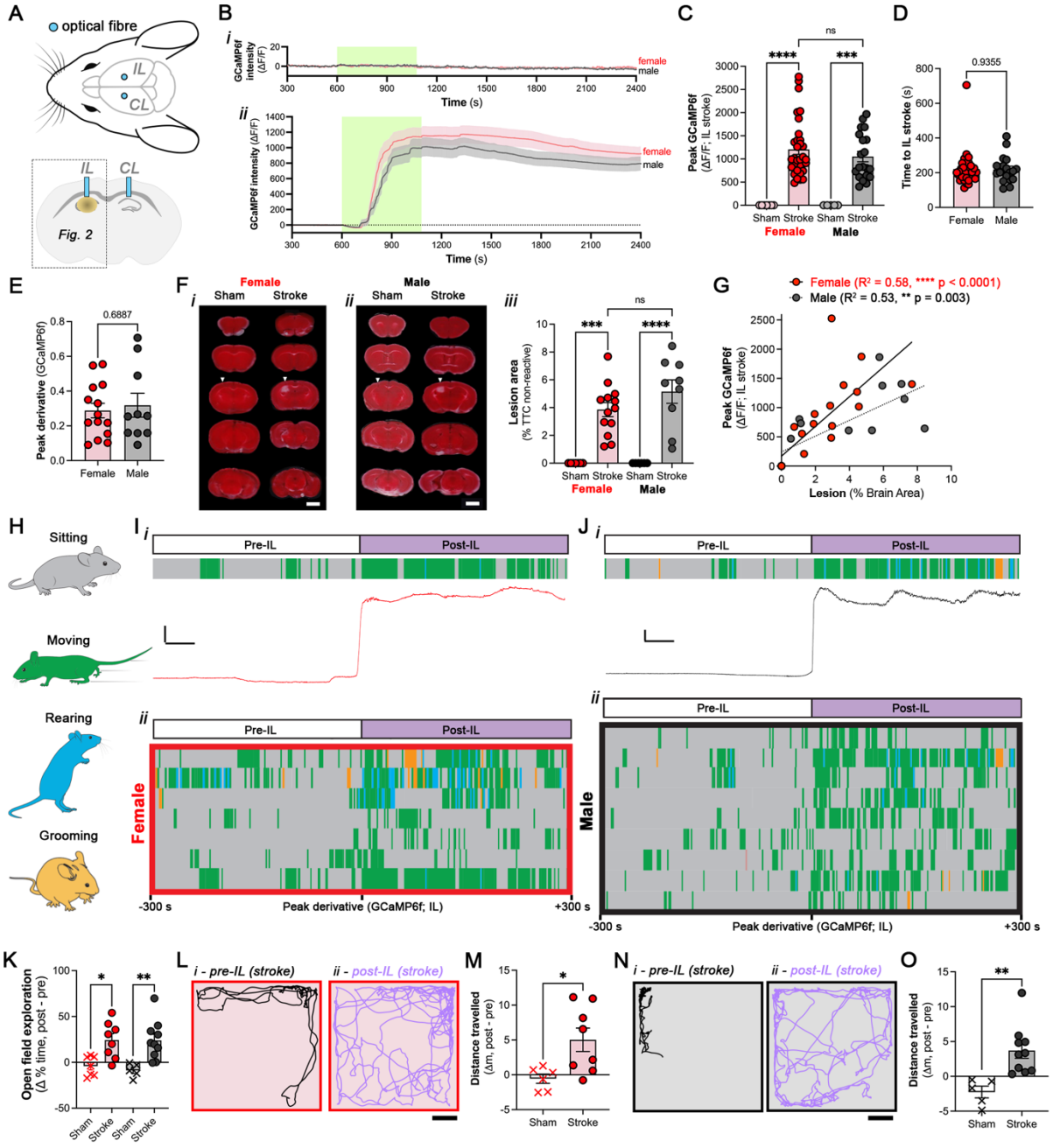

(A) Ipsilesional (IL, Fig. 2) and contralesional (CL, Fig. 3/4) effects of unilateral fiber photothrombotic stroke in the hippocampus. **(B)** Average GCaMP6f intensity (ΔF/F, ***i,*** 100 Hz; mean ± s.e.m.) from ipsilesional optical fiber for female (red) and male (black) sham mice (vehicle, i.p.) during 40 min photometry recording. (***ii***) Neuronal Ca^{2+} dysregulation (GCaMP6f, ΔF/F, mean ± s.e.m.) induced by photothrombosis in female (red) and male (black) stroke mice (1 % RB, i.p.). **(C)** No sex differences between ipsilesional Ca^{2+} dysregulation (peak GCaMP6f, ΔF/F) in hippocampal neurons (female – stroke: 1205 arb. units ± 106.8, n = 32; male – stroke: 1051 arb. units ± 111.7., n = 20, two-way ANOVA with Tukey *post hoc* [sex: $F(1, 61) = 0.20$, $p = 0.65$; sham vs. stroke: $F(1, 61) = 43.74$,**** $p < 0.0001$; interaction: $F(1,61) = 0.20$, $p = 0.65$]).

(D) No sex differences in time to ipsilesional stroke (peak derivative of ipsilesional GCaMP6f; female: 221.5 s ± 18.3, n = 32; male: 219.2 s ± 18.3, n = 20; unpaired t-test). **(E)** No sex differences between peak derivative of ipsilesional Ca^{2+} dysregulation in hippocampal neurons (ipsilesional GCaMP6f, ΔF/F; female: 0.29 ± 0.04, n = 14; male: 0.32 ± 0.07, n = 10; unpaired t-test). **(F)** Stroke induces lesion localized to ipsilesional hippocampus (representative images of TTC-stained coronal sections from sham and stroke brains of (***i***) female (red) and (***ii***) male (black) mice at 48 h post-stroke induction. Arrow indicates the location of the ipsilesional fiber. Scale bars, 2 mm. (***iii***) No sex differences in lesion size between male and female mice following stroke. Two-way ANOVA with Tukey *post hoc* (sex: F(1, 31) = 1.15, p = 0.29; sham vs. stroke: F(1, 31) = 55.42,**** p < 0.0001; interaction: F(1,31) = 1.15, p = 0.29). **(G)** Ipsilesional peak GCaMP6f (ΔF/F) correlatives with lesion size (female: R^2 = 0.57, **** p < 0.0001; male: R^2 = 0.54, ** p = 0.003). **(H)** Behavior state (sitting – grey, moving – green, rearing – blue, and grooming – orange) assessed by overhead camera in open field during peri-stroke period. **(I)** Behavior state (Gantt plot) aligned to a (***i***) representative female ipsilesional neuronal Ca^{2+} dysregulation (peak derivative, ΔF/F, black) demonstrates a time-locked increase in exploration during stroke onset. Scale bar: 100 arb. units, 50 s. (***ii***) Gantt behavioral plots for all analyzed female traces (red) centered on peak derivative of ipsilesional GCaMP6f. Each row represents one mouse (n = 7). **(J)** Behavior state (Gantt plot) aligned to a (***i***) representative male ipsilesional neuronal Ca^{2+} dysregulation (peak derivative, ΔF/F, black) demonstrates a time-locked increase in exploration during stroke onset. Scale bar: 100 arb. units, 50 s. (***ii***) Gantt behavioral plots for all analyzed male traces (black) centered on peak derivative of ipsilesional GCaMP6f. Each row represents one mouse (n = 9). **(K)** Stroke increases time spent exploring (% epoch of either moving or rearing) after ipsilesional Ca^{2+} dysregulation in hippocampal neurons in both females (red, n = 7) and males (black, n = 9). For sham mice, behavioral traces were aligned to the average time of peak derivative (GCaMP6f) in the stroke group (800 s; *see Extended Data Fig 5;* female: n = 7; male, n = 5). Grooming is unchanged in females and males. Two-way ANOVA with Tukey *post hoc* (sex: F(1, 26) = 0.15, p = 0.70; sham vs. stroke: F(1, 26) = 22.32,**** p < 0.0001; interaction: F(1, 26) = 0.11, p = 0.74). **(L)** Example locomotion traces for female mice (red frame) before (*i*, *pre-IL)* and after (*ii, post-IL)* the onset of ipsilesional neuronal Ca^{2+} dysregulation. **(M)** Following ipsilesional neuronal Ca^{2+} dysregulation, females travel further in an open field assay (sham: -0.56 m ± 0.66, n = 7; stroke: +5.01 m ± 1.69, n = 9; unpaired t-test, * p < 0.05). **(N)** Example locomotion traces for male mice (black frame) before (*i*, *pre-IL)* and after (*ii, post-IL)* the onset of ipsilesional neuronal Ca^{2+} dysregulation. **(O)** Following ipsilesional neuronal Ca^{2+} dysregulation, males travel further in an open field assay (sham: -2.26 m ± 0.84, n = 5; stroke: +3.70 m ± 1.11, n = 9; unpaired t-test, ** p < 0.01).

Data Fig. 1). We identified a linear relationship between acute neuronal Ca^{2+} dysregulation and lesion size in both sexes, suggesting neuronal GCaMP6f intensity during the hyperacute phase of stroke could act as a proxy for eventual lesion size (Fig. 2g). This correlation was lost when strokes were performed under anesthesia (Extended Data Fig. 3). Thus, photometry of acute neuronal Ca^{2+} dysregulation in freely behaving mice allows non-histological evaluation of stroke severity (without euthanasia), permitting longitudinal, within-mouse comparisons.

Our model is the first to measure peri-stroke neuronal Ca^{2+} dynamics in freely behaving mice. In sham and stroke mice, we classified behavior into 4 states: sitting, moving, grooming, rearing (Fig. 2h) and evaluated distance travelled using DeepLabCut[30] to identify behavioral change linked to hippocampal stroke onset

(Extended Data Fig. 4). In stroke mice, the time of the peak derivative of GCaMP6f (onset of neuronal Ca^{2+} dysregulation) was identified. Next, the time spent in each behavioral state before and after the onset of neuronal Ca^{2+} dysregulation was assessed (*pre-IL*: -300 to 0 s, and *post-IL*: 0 to +300 s relative to the GCaMP6f peak derivative; Fig. 2*i-j*). For shams, the average onset time of neuronal Ca^{2+} dysregulation in stroke mice was selected to make before/after comparisons (800 s, Extended Data Fig. 5). In female and male stroke, following the onset of neuronal Ca^{2+} dysregulation, mice spent more time exploring the open field (time spent moving or rearing, Fig. 2k) and travelled further (Fig. 2l-o) than shams, who exhibited no change in behavior or distance travelled in an equivalent epoch (Extended Data Fig. 5).

Female mice have larger and more frequent contralesional spreading depolarization-associated Ca^{2+} waves following hippocampal stroke.

The contralesional fiberoptic cannula allowed evaluation of the interhemispheric impacts of stroke in an identical brain region naïve to photothrombotic illumination. Baseline recording from opposing hippocampi revealed no differences in basal GCaMP6f events (Fig. 3ab, Extended Data Fig. 6). Following photothrombotic illumination and ipsilesional neuronal Ca^{2+} dysregulation, a remarkable sex difference appeared in contralesional GCaMP6f dynamics. Large and slow contralesional neuronal Ca^{2+} waves (GCaMP6f) were observed in both sexes (Fig. 3a-c), yet were more frequent, larger, and arrived more rapidly in females (Fig. 3cd, Extended Data Fig. 7). The presence and amplitude of contralesional Ca^{2+} waves had no relationship to the amplitude of ipsilesional neuronal Ca^{2+} dysregulation (Extended Data Fig. 8). The frequency of basal GCaMP6f events was markedly reduced following these contralesional SD waves (Fig. 3e-g) and was negatively correlated to their amplitude (Fig. 3h). While this drop in Ca^{2+} events partially recovered, it did not reach baseline by the end of the recording (up to 40 min, Extended Data Fig. 6). We suspected that these waves were the Ca^{2+} component of interhemispheric spreading depolarizations (SD)[31], given the impact of this wave on photometric readouts of neuronal activity. To test this further, we implanted a bipolar electrode distal to the contralesional fiber in female mice and repeated stroke induction (Fig. 3i-k). Contralesional GCaMP6f waves were strongly associated with hypersynchronous epileptiform activity in AC-coupled local field potential (LFP) recordings followed by a transient suppression of activity (Fig 3k-m), resembling the activity present when spreading depolarization was artificially generated in a hippocampal slice[32].

Female mice increase exploration during and after contralesional spreading depolarization.

The potential for a behavioral link to contralesional Ca^{2+} waves was explored. For shams, no change in behavior or locomotion occurred around the average time of

Figure 3. Female mice have larger and more frequent contralesional spreading depolarizations following hippocampal stroke.

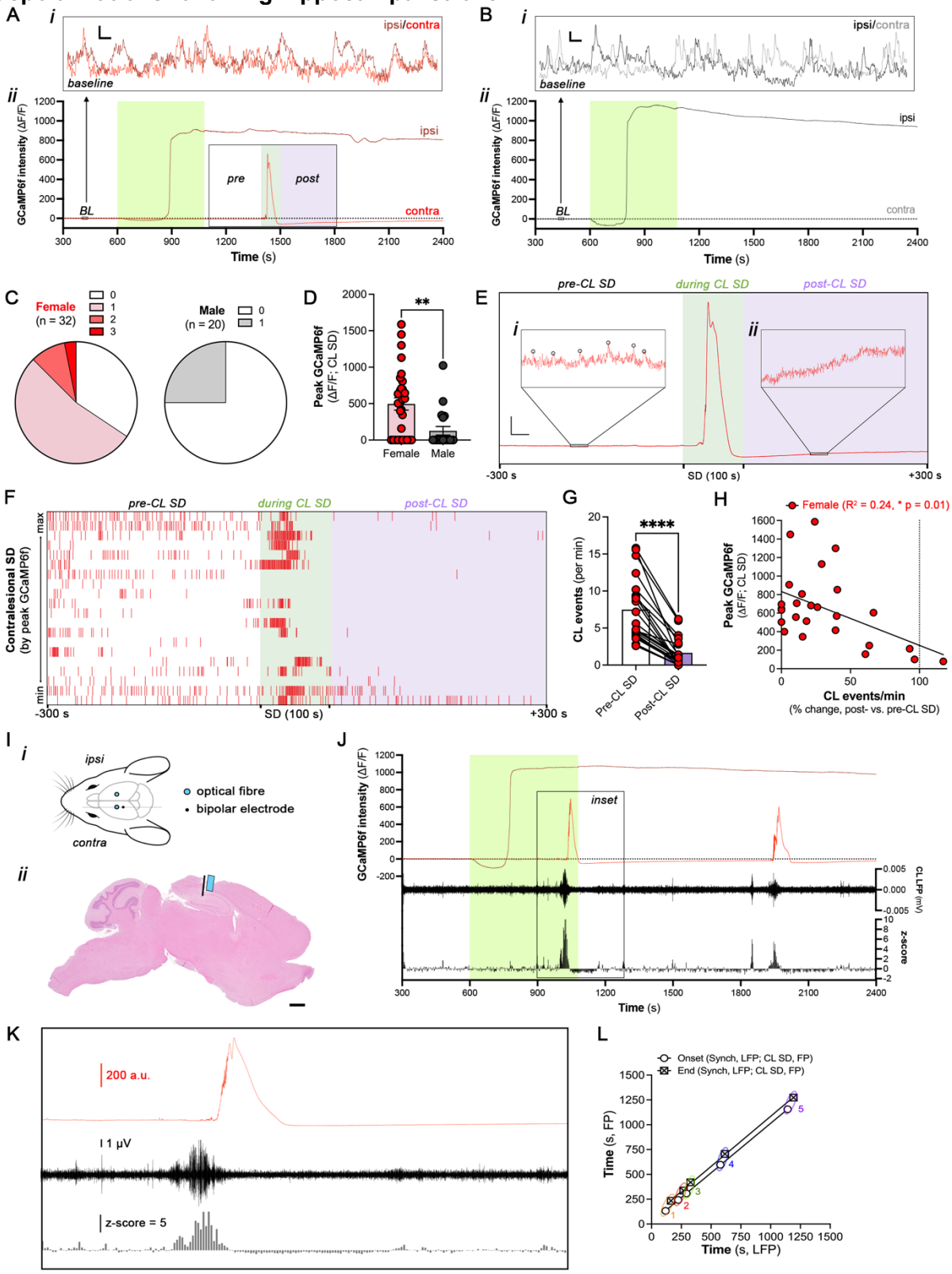

(A) Representative *(i)* baseline (scale bar: 1 arb. units, 1 s) and ***(ii)*** total (300 – 2400 s) ipsilesional (dark red) and contralesional (light red) GCaMP6f photometry traces (ΔF/F) in awake and freely-behaving female mice during stroke. Photothrombosis induction (561 nm, 6 mW, 600-1080 s, green box). Contralesional spreading depolarization (CL SD) associated GCaMP6f wave highlight (box) with pre-, during, post epochs. **(B)** Representative ***(i)*** baseline (scale bar: 1 arb. units, 1 s) and ***(ii)*** total ipsilesional (black) and contralesional (grey) GCaMP6f photometry traces, conditions as above, in male mice during stroke. **(C)** Pie charts indicating number of CL SD in female (red, n = 32) and male (black, n = 20) mice post stroke. **(D)** Females have larger Ca^{2+} dysregulation (peak GCaMP6f, ΔF/F) during CL SD (female: 495.2 arb. units ± 85.25, n = 32; male: 126.1 arb. units ± 59.1, n = 20; Mann-Whitney, ** p = 0.0012). **(E)** Representative female contralateral Ca^{2+} wave highlights reduction of basal Ca^{2+} events following large transient increase in GCaMP6f. Scale bar: 200 arb. units, 30 s. (***i***) Pre-CL SD Ca^{2+} event (circled, peaks > 4 STD of mean, separated by > 0.5 s;) are absent in (***ii***) post-CL SD photometry recording (frames: 15 arb. units, 30 s). **(F)** Ca^{2+} events (raster plot) decrease after CL SD. Each row represents an individual CL SD (n = 21). **(G)** Contralateral Ca^{2+} events per min are reduced following CL SD-associated Ca^{2+} wave. (pre-CL SD: 7.49 ± 0.93, post CL-SD: 1.65 ± 0.42, n = 21; paired t-test, **** p < 0.0001.). **(H)** Contralesional SD (peak GCaMP6f, ΔF/F) negatively correlates with the change (%) in Ca^{2+} events/min following the SD (female: R^2 = 0.24, * p = 0.01, n = 21). **(I)** Schematic of ***(i)*** CA1-targeted bilateral fiberoptic cannulas (blue) and contralesional bipolar electrode implant (black). *(ii)* Representative hematoxylin and eosin (H&E) stained sagittal section of Thy1GCaMP6f mouse (contralesional hemisphere) at fibre and electrode implant locus one-week post-stroke. Scale bar, 2 mm. **(J)** Example ipsilesional (dark red) and contralesional (light red) GCaMP6f (ΔF/F) paired with contralesional LFP (black trace) in an awake, behaving female mouse. Z-score (bar graph, bottom) of binned LFP trace (2 s bins) indicates depression of activity following onset of CL SD. Laser illumination to evoke thrombosis (561 nm, 6 mW, 8 min, green box). Inset box encapsulates a 400 s period surrounding the onset and end of synchronous activity in LFP and the first contralesional spreading depolarization (CL SD, GCaMP6f). **(K)** Expanded *Fig 3k (inset)* highlights epileptiform activity (LFP) that precedes the onset of CL SD (GCaMP6f) followed by depression in activity. Scale bars in descending order, 200 arb. units, 1 μV, z-score = 2. **(L)** Onset (empty circle) and end (hatched box) of synchronous contralesional activity (LFP, x-axis) and CL SD-associated Ca^{2+} wave (GCaMP6f FP, y-axis) in the hippocampus following fiber photothrombotic stroke is strongly correlated. Linear regression (onset: R^2 = 0.99, **** p < 0.0001; end: R^2 = 0.99, **** p < 0.0001; n = 5 CL SDs from 4 female mice).

contralesional Ca^{2+} waves in stroke mice (1400 s, Extended Data Fig. 9). In stroke, we classified behavior before, during, and after contralesional SD-associated Ca^{2+} waves (*pre-SD*: -350 to -50 s relative to, *during*: 100 s surrounding, and *post-SD*: +50 to +350 s relative to center of Ca^{2+} wave, respectively; Fig. 4a-b). Females spent more time exploring the open field both during and after contralesional Ca^{2+} waves (Fig. 4c), however no difference was observed in males (Fig. 4d). While contralesional Ca^{2+} waves were followed by increased exploration, the amplitude of these waves was strongly correlated to reduced exploration during the wave (Fig. 4e). This could be the result of increased synchronous electrical activity with larger waves, eliciting tonicity in mice. Finally, while average speed was not significantly different during the contralesional Ca^{2+} waves, female mice moved faster in the *post-CL* epoch (Fig. 4f-g). Males showed no change in average speed in relation to their contralesional Ca^{2+}

waves (Fig. 4h-i). Taken together, following hippocampal stroke, females displayed unique contralesional Ca^{2+} transients and accompanying increased exploration.

Figure 4. Female mice increase exploration during and after contralesional spreading depolarization.

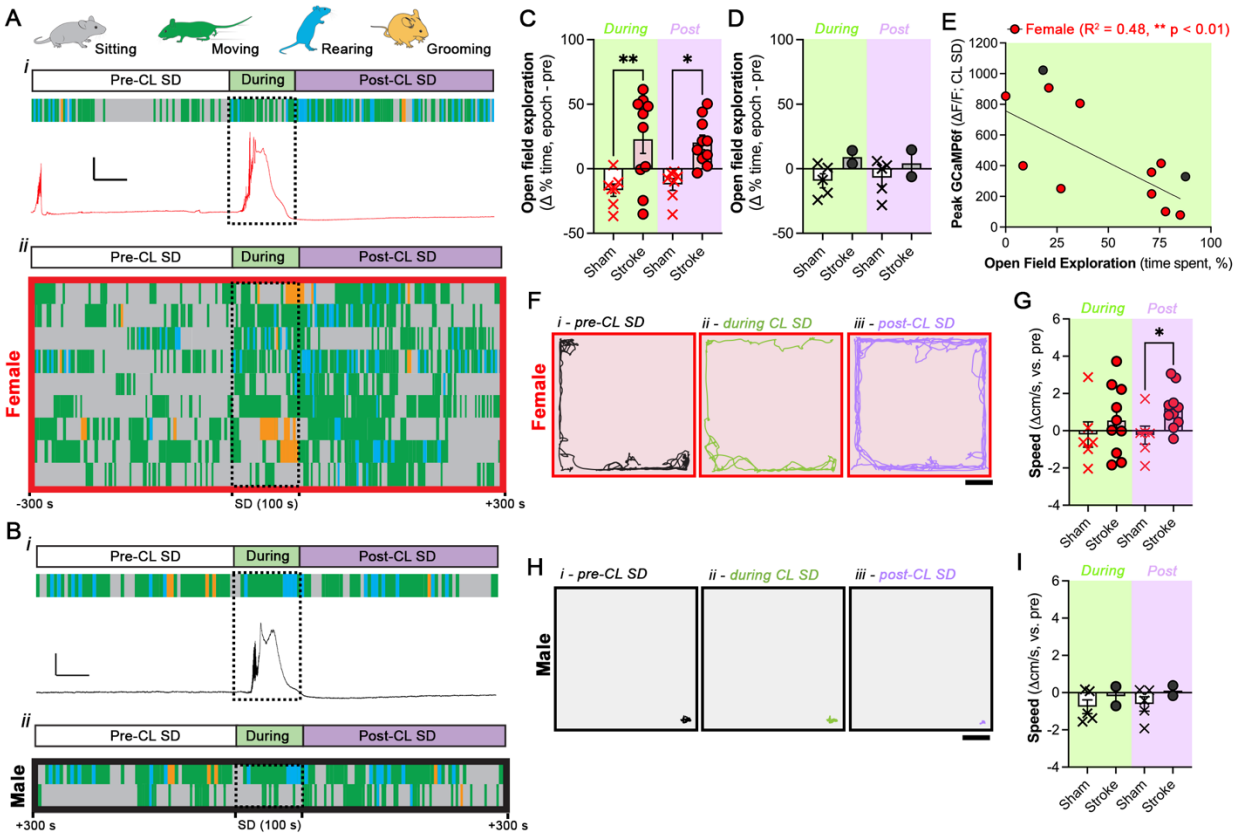

(A) Behavior state (***i***, Gantt plot; sitting – grey, moving – green, rearing – blue, and grooming – orange) aligned to a representative female contralesional spreading depolarization (CL SD, GCaMP6f, ΔF/F, red) demonstrates increased exploration during/after CL SD. Scale bar: 100 arb. units, 50 s. (***ii***) Gantt behavioral plots for all analyzed female traces (red) centered on CL SD. Each row represents one mouse. **(B)** Behavior state (***i***) aligned to a representative male CL SD. Scale bar: 100 arb. units, 50 s (*ii*) Gantt behavioral plots for all analyzed male traces (black) centered on CL SD. Each row represents one mouse. **(C)** Females increase time spent exploring the open field (% of epoch moving or rearing) during and after CL SD (sham – during: -16.6% ± 4.75, n = 6; stroke – during: +22.89% ± 11.0, n = 10; sham – post: -12.14% ± 4.5, n = 6; stroke – post: +20.4% ± 5.61, n = 10; unpaired t-tests, ** $p < 0.01$, * $p < 0.05$). **(D)** Male exploration is unaffected by CL SD (sham – during: -9.31% ± 5.4, n = 5; stroke – during: +9.1% ± 5.1, n = 2; sham – post: -6.94% ± 6.43, n = 5; stroke – post: +4.26% ± 10.34, n = 2; unpaired t-tests). **(E)** Contralesional SD amplitude (ΔF/F) is negatively correlated to time spent exploring during CL SD (female: $R^2 = 0.48$, ** $p < 0.01$). **(F)** Locomotion traces before (***i***, *pre-CL), during* ***(ii)*** and after (*iii, post-CL)* CL SD in a representative female (red frame). **(G)** Average locomotion speed is unchanged during CL SD yet increases following CL SD in females. (sham – during: -

0.002 m/s ± 0.007, n = 6; stroke – during: 0.006 m/s ± 0.006, n = 10; sham – post: -0.002 m/s ± 0.0.005, n = 6; stroke – post: 0.01 m/s ± 0.003, n = 10; unpaired t-tests, * $p < 0.05$). **(H)** Locomotion traces (***i***) before, (***ii***) during, and (***iii***) after CL SD in a representative male (black frame). **(I)** Average locomotion speed is unchanged during and after CL SD in males (sham – during: -0.01 m/s ± 0.003, n = 5; stroke – during: -0.002 m/s ± 0.005, n = 2; sham – post: -0.006 m/s ± 0.0.003, n = 5; stroke – post: 0.001 m/s ± 0.003, n = 2; unpaired t-tests).

Contralesional spreading depolarization abrogates memory impairment following hippocampal stroke.

While presumed deleterious in hypoperfused penumbral tissue, the impact of spreading depolarization through remote tissue is less understood[14]. We first assessed the impact of unilateral hippocampal stroke and SD-associated Ca^{2+} waves on retrograde (Fig. 5a-b) using contextual fear conditioning, a hippocampus-dependent task[33–35]. To assess retrograde amnesia, mice were subjected to 3 foot shocks in a novel context prior to hippocampal stroke (~10 min; Fig. 5a). After 24 h, mice were returned to the same context. Female and male shams increased freezing on day 2 (Fig. 5a), suggesting preserved fear memory retrieval. Meanwhile, stroke abolished freezing, indicating retrograde amnesia (impaired contextual fear conditioning). Freezing in stroke mice was negatively correlated to the amplitude of ipsilesional Ca^{2+} dysregulation and unimpacted by contralesional Ca^{2+} waves (Fig. 5b).

One week after stroke, mice were again subjected to contextual fear conditioning, this time to assess their ability to form and retrieve new contextual fear memories to determine if anterograde amnesia was present (Fig. 5c-d). Mice were returned to the foot shock chamber and 3 foot shocks were delivered over a period of 7 min. When returned to the identical context, following a second round of foot shocks, only stroke mice that had displayed contralesional Ca^{2+} waves during stroke the week prior showed significant freezing. This effect was strongest in females, who recovered to sham levels (Fig. 5c), providing evidence that contralesional Ca^{2+} waves were protective against anterograde amnesia triggered by unilateral hippocampal stroke. Freezing during this task was correlated to the amplitude of the contralesional waves (Fig. 5d). Finally, freezing was specific to the fear conditioned context, as neither sham nor stroke mice increased freezing in a novel context absent of foot shock (Extended Data Fig. 10).

Discussion

Clinical translation of stroke therapeutics has seen an overwhelming number of failures[36], tormented by the lack of an animal model of stroke that closely relates to human disease. While major leaps have been made in previous years allowing less invasive stroke protocols in awake mice, here we present the first model for stroke induction in a freely behaving mouse with simultaneous recording of neuronal Ca^{2+} dysregulation. We take advantage of permanent bilateral fiberoptic cannulas to both

induce unilateral stroke using photothrombosis in the hippocampus and bilaterally record neuronal Ca^{2+} via GCaMP6f fluorescence in Thy1-GCaMP6f mice. This protocol requires no surgery or anesthetic on the day of stroke induction, avoiding the neuroprotective effects of anesthesia in the peri-stroke period.

Figure 5. Contralesional spreading depolarization abrogates memory impairment following hippocampal stroke.

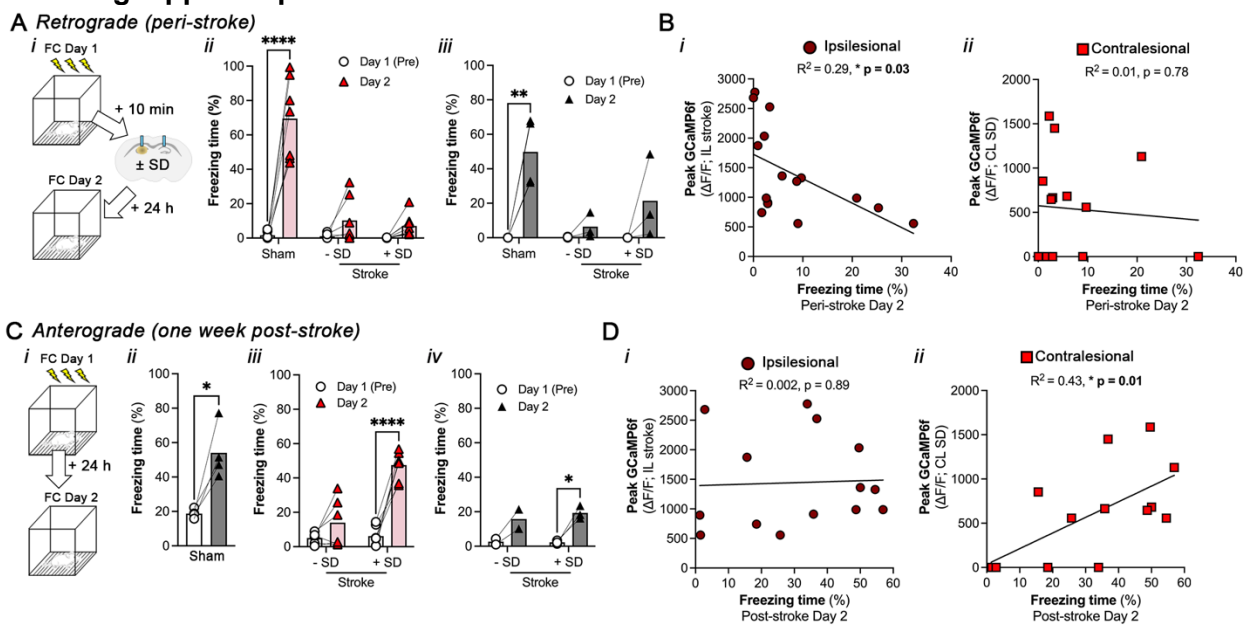

(A) Schematic (***i***) of contextual fear conditioning to assess retrograde amnesia following stroke. Day 1: 3 evenly spaced foot shocks (FS, Context 1, 7 min) followed by stroke induction in open field, 10 min post-FS. Day 2: mice are returned to Context 1 without FS (7 min). Stroke induces retrograde amnesia in (***ii***) female (two-way RM ANOVA with Bonferroni *post hoc* [time: $F(1,19) = 69.59$, **** $p < 0.0001$; insult: $F(2, 19) = 37.41$, **** $p < 0.0001$; interaction: $F(2, 19) = 34.68$, **** $p < 0.0001$]) and (***iii***) male mice (two-way RM ANOVA with Bonferroni *post hoc* [time: $F(1,7) = 18.44$, ** $p < 0.01$; insult: $F(2, 7) = 4.8$, * $p < 0.05$; interaction: $F(2, 7) = 4.92$, * $p < 0.05$]). Percentage of total time spent freezing in Day 1 (pre-shock, white circle) and Day 2 (triangle) for female sham and stroke mice with or without SD (-SD or +SD, respectively). **(B)** Ipsilesional neuronal Ca^{2+} dysregulation (***i***, peak GCaMP6f, $\Delta F/F$) negatively correlates with time spent freezing during retrieval in females (%, Day 2 – Context 1; $R^2 = 0.29$, * $p = 0.03$). (***ii***) No correlation exists between contralesional SD amplitude and time spent freezing during retrograde amnesia assay in females ($R^2 = 0.01$, $p = 0.78$). **(C)** Schematic (***i***) of contextual fear conditioning assay to assess anterograde amnesia one week after stroke. Day 1: 3 evenly spaced foot shocks (FS, Context 1, 7 min). Day 2, mice are returned to Context 1 without FS (7 min). Fear conditioning is successful in (***ii***) sham mice one week following illumination (561 nm). Time spent freezing (%) is increased in Day 2 (triangles), relative to Day 1 (white circle) prior to FS (paired t-test, * $p < 0.05$). (***iii***) CL SD in females reduces stroke-induced anterograde amnesia to sham levels in a fear conditioning test one-week post-stroke (Freezing time, %). Two-way RM ANOVA with Bonferroni *post hoc,* time: $F(1,11) = 60.82$, **** $p < 0.0001$; insult: $F(1, 11) = 23.94$, *** $p = 0.0005$; interaction: $F(1, 11) = 25.27$, *** $p = 0.0004$. (***iv***) CL SD in males reduces stroke-induced anterograde amnesia (Freezing time, %). Two-way RM ANOVA with Bonferroni *post hoc*, time: $F(1,3) = 44.03$, ** $p = 0.007$; insult: $F(1, 3) = 0.29$, $p = 0.63$;

interaction: F(1, 3) = 0.74, p = 0.45.**(D)** Ipsilesional neuronal Ca^{2+} dysregulation (***i***, peak GCaMP6f, ∆F/F) is not correlated with time spent freezing during retrieval in females (%, Day 2 – Context 1; R^2 = 0.002, * p = 0.89). (***ii***) Contralesional SD amplitude (peak GCaMP6f, ∆F/F) correlates with reduced anterograde amnesia in females (% freezing, Day 2, one week post-stroke; R^2 = 0.43, * p = 0.01).

Plenty of attention has been given to modelling focal ischemic stroke in the superficial cortex using photothrombosis[26,27,37] and magnetic nanoparticles[28], yet less has been given to developing models for stroke in deeper brain structures. There are several other models where stroke encroaches on or is targeted to deeper structures, each with unique benefits and limitations. Intralumenal middle cerebral artery occlusion (MCAO) induces a large lesion that spreads primarily into superficial neocortex, yet reaches some deeper subcortical regions[25], however MCAO requires anesthesia, and any impairments are difficult to link to specific structures. Injection of thromboemboli or microspheres can induce subcortical stroke[38], however this creates unpredictable infarcts distributed diffusely throughout the brain. Optical fibers have been used for photothrombosis in deeper structures including the internal capsule[39], caudoputamen[40], and hippocampus[41], yet none of these studies have paired stroke induction (photo-oxidation) with an acute stroke readout (photometry) or used awake mice, as in this study. A chronic fiberoptic implant allows mice to freely behave, making available an array of brain region-specific behavioral tasks. Not only does this approach permit stroke induction in understudied brain regions, but it also provides access to real time region-specific neuronal activity and correlation to peri-stroke behavior. This is particularly important, as sex differences have been observed in symptom presentation in humans post-stroke[2], which has led to increased rates of misdiagnosis in women, and consequently, fewer women receiving thrombolysis in the critical therapeutic window[3,4].

The main feature of unilateral hippocampal stroke in humans is disorientation, which typically resolves in a weeks following stroke[42]. In the present study, unilateral hippocampal stroke in mice was associated with increased exploration during and immediately following the onset of neuronal Ca^{2+} dysregulation, which was distinct from behavior induced by focal cortical stroke in a previous study[26]. MCAO occlusion induced hypoactivity in mice at the time of photo-activation, an approximation of stroke onset[26]. This provides evidence that, like longitudinal cognitive and behavioral impairments[43], hyperacute behavioral effects are region-specific. Increased open field exploration following a hippocampal stroke might be caused by impaired spatial memory formation, reintroducing a “novel” environment, and slowing habituation[44]. A caveat of previous studies looking at peri-stroke behaviors is the absence of a real-time readout of stroke onset; thus, the peri-stroke epoch was approximated. Moving forward, combined photometry and photothrombosis will allow precise interrogation of hyperacute stroke-induced behavior and how peri-stroke behavior impacts stroke outcome.

While ipsilesional neuronal Ca^{2+} dysregulation and related behavior were not different between sexes, contralesional Ca^{2+} dynamics and linked behavior were sexually distinct. We observed sex differences in contralateral SD frequency following unilateral ischemic stroke in the hippocampus. In cortical SD, waves are typically limited to the ipsilesional hemisphere; however, in Leão's seminal study, contralateral SD was observed at symmetrical loci, yet contralateral SD were smaller, covered a smaller area, and were non-coincident with the ipsilateral SD[7]. SDs were more likely to appear in the opposite hemisphere if they were evoked in more anterior cortex. In neocortical SD, contralateral spread is thought to be limited by a transcallosal inhibitory effect[45] mediated, at least in part, by voltage-gated potassium channels[46], which are localized to the axon initial segment[47,48]. In Kv1.1-KO mice, following the unilateral injection of a chemoconvulsant, the acute inhibition of Kv7 produced symmetric bi-hemispheric SDs that were otherwise limited to the targeted hemisphere[46]. It remains possible that the common observation of ipsilesionally contained SD is an experimental bias, as the neocortex is more accessible to induction and monitoring of SD. Our model will now permit direct observation of where and when SD spreads when stroke occurs in deeper structures of the non-anesthetized brain.

Here, we present sex differences in response to disease-related induction of SD (focal ischemia); however, sex differences in SD susceptibility have been shown in response to topical application of potassium chloride to artificially induce SD on the neocortex[49]. Females exhibited increased frequency of SD relative to males. Gonadectomy in females eliminated this sex difference. In gonadectomized females, estrogen withdrawal after prolonged daily treatment or, conversely, daily injection of progesterone increased CSD susceptibility, while this effect was not observed in males[49]. This suggests that estrogen and progesterone could play a role in propagation of spreading depolarization into the contralesional hippocampus in our model.

We observed an increase in exploration during the onset of SD-associated Ca^{2+} waves in the contralateral hippocampus. This is consistent with previous studies using optogenetic activation of channelrhodopsin in cortical pyramidal neurons (Thy1-ChR2) to generate SD in otherwise healthy tissue. In this case, a peak in locomotor activity was observed immediately following the induction of SD, once it had reached the primary motor cortex, where electrical activity was being recorded[50]. It is possible in our case, that SD is also reaching motor areas to elicit locomotion directly. It may also be the case that strong depolarization of hippocampal neurons indirectly evokes locomotor activity. While not directly involved in inducing motor activity, the hippocampus can influence running speed[51,52] and regulate spatial memory[53] allowing for navigation strategies in space. A stroke model in freely behaving mice will now permit interrogation of how modulating behavior in the hyperacute period might feedback onto SD generation and stroke outcomes.

While unilateral hippocampal stroke generated retrograde amnesia in a contextual fear conditioning assay (Fig. 5ab), we observed a striking reduction in anterograde amnesia in mice that had contralesional SD following stroke a week prior to evaluation (Fig. 5cd). Reduction of anterograde amnesia correlated with the amplitude of contralesional SD but had no relationship to ipsilesional neuronal Ca^{2+} dysregulation. It is possible that SD, observed in the contralesional hippocampus in the present study, is upregulating plasticity-inducing or neurogenic factors as has been observed in other models[16–20]. While one week post-stroke is too short for newly generated cells to integrate into a hippocampal circuit[54], it is possible that SD could bolster plasticity/integration of existing hippocampal neuronal and glial progenitors or support plasticity in existing hippocampal circuits.

Taken together, we present a stroke model for both inducing ischemic stroke and recording subsequent neuronal Ca^{2+} dysregulation in awake, freely behaving mice. Symmetric bilateral fiberoptic cannulas targeting the CA1 in Thy1GCaMP6f mice revealed sexually indistinct ipsilesional neuronal Ca^{2+} dysregulation and associated behavior yet revealed a strong sex difference in contralesional spreading depolarization associated Ca^{2+} waves. These waves induced increased exploration upon arrival, but also had longitudinal impacts on learning and memory, as indicated by a reduction in anterograde amnesia during contextual fear conditioning. This model opens the door for using fiber photometry in pathological settings and offers a unique perspective on stroke biology in a freely behaving animal. Future studies could consider using other biosensors or exploring other cell types using the same technology to get a deeper analysis of how stroke-related biology is linked to peri-stroke behavior.

Methods

Animals

All animal care protocols were in accordance with the Canadian Council on Animal Care guidelines and approved by the University of Calgary's Animal Care and Use Committees. Both Thy1GCaMP6f (C57BL/6J-Tg(Thy1-GCaMP6f)GP5.17Dkim/J, JAX 025393)[24] female and male mouse littermates from Thy1GCaMP6f(+/-) breeding pairs were group housed until the first procedure and then single housed on a 12 h/12 h light/dark cycle. Mice had *ad libitum* access to Purina laboratory chow and water.

Fiberoptic implant

Thy1GCaMP6f mice (P60-120, N = 65, 32 awake bilateral females, 20 awake bilateral males, 5 awake unilateral males, 8 anesthetized unilateral males) were anesthetized using inhaled isoflurane (5% induction; 1% maintenance) for surgery, then placed in a stereotaxic apparatus. Next, the area above the skull was shaved to expose the scalp and a midline incision (~3 cm) was made. The skull was exposed by detaching the muscle from the sagittal ridge then cleaned using 5% hydrogen peroxide. Bregma and

lambda were located and equilibrated in the dorsal ventral plane. From here, mono-fiberoptic cannulas (Doric Lenses) were implanted dorsal to the CA1 region of each hippocampus (AP -2.0 mm, ML ±1.3 mm from bregma, and DV -1.0 mm from the brain surface) and were fixed to the skull using serial application of Metabond and dental cement. Where applicable, Secondary burr holes were made for bipolar depth electrodes to simultaneously record local field potentials (LFPs) in contralesional hippocampus. Electrodes were constructed from a 178 μm stainless steel wire connected to gold-plated male amphenol pins (A-M systems) and lowered at stereotaxic coordinates: (right: AP -2.30, ML +1.3 mm from bregma, DV -1.5 mm from surface; left: AP -2.30, ML -1.3mm from bregma, DV -1.5 mm from surface). Mice were allowed to recover for 7 days prior to *in vivo* stroke.

Photothrombotic stroke & fiber photometry in awake and freely behaving mice

For focal ischemia in the hippocampus (photothrombosis, Watson *et al.*, Ann Neurol, 1985) in awake and behaving mice, the mice were administered vehicle (PBS pH 7.2, 0 $MgCl_2$, 0 $CaCl_2$; Invitrogen Cat. 20012050) or Rose Bengal (1% w/v in PBS; Sigma Canada R3877-5G) via intraperitoneal injection (0.1 mL per 10 g of bodyweight) 15 minutes prior to the onset of photothrombosis. Solutions were freshly prepared, sonicated, then sterile filtered immediately prior to use. Anesthetized mice were maintained under isoflurane anesthesia for the duration of the experiment (induction: 5%, maintenance: 1%). The light source (for photothrombosis; 561 nm, LRS-0561-GFO-00100-03, LaserGlow Technologies) was connected to the implanted ferrule (400 μm core diameter, MFC_400/430-0.48_2.5 mm_MF2.5_FLT, Doric Lenses). Brain volumes immediately below the fiberoptic cannula were illuminated for 1.5 or 8 min with 4, 5, or 6 mW intensity, where indicated.

Neuronal calcium (GCaMP6f) in ipsilesional and contralesional CA1 from freely behaving Thy1-GCAMP6f mice was recorded using fiber photometry for 40 minutes surrounding the induction of photothrombosis (10 minutes prior to 561 nm illumination, 30 minutes following onset of illumination). Mice were excluded from the study if no GCaMP6f events were observed during baseline (GCaMP6f-negative, n = 3).

To record neuronal GCaMP6f, a Doric fiber photometry system was used, consisting of two excitation LEDs (405 nm and 465 nm, 30 μW) controlled by the LED driver and console running DoricStudio software (Doric). Both modulated LEDs (lock-in amplification) and the 561 nm laser were filtered through a Doric Mini Cube filter set (FMC6_IE(400-410)_E1(460-490)_F1(500-540)_E2(555-570)_F2(580-880)_S) with the excitation light directed to the implanted cannula using a mono fiberoptic patchcord (Doric MFP_400/460/900-0.48_2m_FC/MF2.5). Emitted fluorescence signal between 500-540 nm was then demodulated using lock-in amplification and detected by a photoreceiver (NewPort model 2151). Following stroke, mice were followed for behavior analysis, or sacrificed for lesion histology at 48 h or 7 days post-stroke.

Fiber photometry data analysis

Frequency-modulated GCaMP6f fluorescence (405-/465-nm excitation) was acquired at a sampling rate of 1 kHz and resampled to 100 Hz in the DoricStudio software. These data were then exported to MATLAB R2023a (Mathworks) for analyses using a custom-written script. Here, an exponential decay was fit to then removed from both the 405 and 465 signals to account for any photobleaching-related artifacts. Motion artifacts in the photometry trace were removed by subtracting the Ca^{2+}-independent 405-nm channel from the Ca^{2+}-dependent 465-nm channel. The output of these transformations generated a motion-corrected dataset for change in GCaMP6f fluorescence. High frequency components of the trace were removed by smoothing the signal to 10 Hz. To normalize data between sessions, we normalized the signal using a modified z-score: $\Delta F/F = (F-F_0)/\sigma F$, where F is the signal, F_0 is the median signal, and σF is the median absolute deviation of the signal. For peak GCaMP6f analyses, a low-pass filter (0.1 Hz) was used, and dysregulation was determined when $\Delta F/F > 20$. Peak GCaMP6f was the maximum intensity value across the 2400 s recording.

To estimate the peak derivative of the GCaMP6f signal for mouse i, $x^i(t)$, the signal was first smoothed with a lowess smoothing filter and with a 10 second window, as implemented by the MATLAB (2023a) function *smooth*. This creates a smooth estimate, $x_s^i(t)$ of the signal $x^i(t)$ which filters much of the high-frequency jitter common in experimentally recorded signals. The derivative was then estimated with the first order finite-difference approximation:

$$\frac{dx_s^i(t)}{dt} = \frac{x_s^i(t+\Delta) - x_s^i(t)}{\Delta}$$

Where $\Delta = 0.05$ seconds is the sampling frequency of the recordings. The approximation to the derivative was used to determine when the GCaMP6f signal had its maximal rise time, defined by:

$$t_i^* = \underset{t}{argmax}\ \frac{dx_s^i(t)}{dt}$$

To avoid boundary effects, the derivatives $\frac{dx_s^i(t)}{dt}$ were manually set to zero in the first and last 5 seconds of recordings.

Local field potential recording and analysis

Neuronal activity was recorded at 512 Hz using an AC amplifier (A-M systems) and collected using DATAQ acquisition software. These traces were post-processed digitally using Curry 8 (Compumedics Neuroscan). Filtering was done using a 60 Hz notch filter to non-selectively remove 60 Hz artificial noise. Traces were then put through a finite impulse response filter to filter low pass at 32 Hz and high pass at 80 Hz. Z-score in relation to the mean for the contralesional LFP trace was assessed in 2 second time bins over the course of the recording. Seizure epochs were identified and binned accordingly to qualify temporal dynamics in relation calcium transients.

Peri-stroke open field behavioral state analysis

Mice were handled (>5 min per mouse) for the four days preceding stroke, including a 1 h habituation period in the experimental room prior to the onset of the experiment. Position of the mouse time-locked to photometry was captured in an open field (0.5 x 0.5 m) using an overhead camera recording at 20 fps. Video analysis of behavioral state was conducted blind to the experimental conditions using a macro for Microsoft Excel (see [55]). Sitting was defined when the mouse made no movement around its environment. Moving was identified when the mouse changed its location or when its hands shifted during a turn in position. Rearing was defined when the mouse stood up on its hindlegs and contacted the wall of the open field. Grooming occurred when the mouse used its hands to clean itself. Normalized photometry signal ($\Delta F/F$; downsampled to 20 Hz) was then aligned to behavioral state data over the duration of the recording (2400 s) and exported to MATLAB for analyses using a custom-written script. For stroke mice, the average time spent by each mouse in each behavioral state was determined for the intervals in before (-300, 0 s) and after (0,300 s) the peak-derivative of ipsilesional GCaMP6f (*pre-IL, post-IL,* respectively). Behavioral states over time were displayed in the form of a horizontal Gantt plot, where GCaMP6f signal and behavioral state Gantt plots were shifted in time so that all mice within a group were each aligned to their own peak rise of the GCaMP6f signal. In shams, GCaMP6f did not display a large change in amplitude, as such, behavioral states were compared in two 300 second intervals before/after the average time of ipsilesional peak derivative in the stroke group (onset of neuronal Ca^{2+} dysregulation, 800 s). For behavioral state linked to contralesional spreading depolarization associated Ca^{2+} waves, a 100 s epoch encompassing the contralesional Ca^{2+} wave (where $\Delta F/F > 20$) was used as the *during* epoch. The 300 s period before and after the *during* epoch were used as the *pre-CL SD* and *post-CL SD* epochs, respectively. For shams, the average time of where GCaMP6f peaked during CL SD in stroke mice (1350-1450 s) was used to center the *pre-CL, during,* and *post-CL* epochs. Moving and rearing were combined to determine time spent exploring.

Positional analyses

Position data were obtained by annotating the center of mass of the mouse in 20-40 frames per training video using DeepLabCut[30] to then predict the position for all video frames for all recordings, then low-pass filtered below 10 Hz using a 9-order Chebyshev type 2 filter to remove high frequency noise. Distance travelled was determined for sham and stroke mice in *pre-IL* and *post-IL* epochs, as defined in Behavioral State analysis, and the difference in total distance was subtracted to relative locomotion. Contralesional analysis used epochs of different absolute times, therefore average speed was used as a metric of locomotion. Here, distance travelled during *pre-CL,*

during, and *post-CL* epochs was divided by time (s) of each epoch; difference in speed was then compared to *pre-CL* epoch.

Contextual fear conditioning

Contextual fear conditioning was evaluated using ANY-maze Video Tracking software. On Day 1, 10 minutes prior to induction of stroke or sham, mice were placed into context 1 (transparent walls, metal grate floor, 80 lumens) where they received 3 foot shocks evenly spaced over 7 minutes (t = 140 s, t = 280 s, t = 520 s). Mice were returned to context 1 at 24 h post-stroke for 7 minutes absent of stroke. Percentage of time freezing (Freezing score < 50 for > 250 ms) was compared between sham and stroke (± SD) for the epoch prior to the initial foot shock on Day 1 (pre-shock) relative to freezing throughout Day 2 (Round 1, retrograde amnesia). At 48 h post-stroke, mice were placed into Context 2 (black striped walls, white plastic floor) for 7 minutes absent of foot shock to evaluate presence of freezing in novel context. At 6 days post-stroke, mice were placed in Context 1 and three evenly spaced foot shocks were administered over a 7-minute interval. At 7 days post-stroke, mice were returned to Context 1 absent of foot shocks. Percentage of time freezing was compared between sham and stroke (± SD) between Day 1 pre-shock relative to throughout Day 2 (Round 2, anterograde amnesia). At 8 days post-stroke, mice were placed into Context 3 (grey walls, black plastic floor) for 7 minutes absent of foot shock. Data were presented as percentage of time spent freezing during given epoch.

Lesion histology

At 48 h post stroke, brain tissue viability was assessed using a macroscopic live-dead stain, triphenyltetrazolium chloride (TTC). Briefly, mice were anesthetized using inhaled isoflurane, decapitated, and brains extracted into ice-cold saline for 5 min. Coronal slices (2 mm) were made using a BrainBlock (Zivic Instruments), then placed in a 1% TTC solution for 30 min at 37 ˚C. Slices were then moved to 4% paraformaldehyde (PFA) for 24 h prior to imaging. Digital images were acquired with a desktop color scanner (600 dpi) and lesion area (white) relative to healthy tissue (red) was analyzed using FIJI. At 7 days post stroke, brains were collected to determine the histological profile of the lesion for each experimental group. Mice were injected with sodium pentobarbital (30 mg/kg, i.p.) then transcardially perfused with saline and 4 % PFA in succession. Extracted brains were placed in 4 % PFA for > 24 h, then in 30% sucrose in PBS at 4 ˚C. After fixation, 40 µm thick brain slices were collected in the region surrounding the fiberoptic implant for both control and stroke experimental groups using a cryostat and mounted on slides (Fisher Scientific). Slices were rehydrated in PBS, permeabilized with 0.3 % Triton-X (PBS-Tx) for 10 min, then blocked in 10 % normal goat serum (NGS) in PBS-Tx for 1 h. Slices were incubated in anti-Iba1 (1:500, Invitrogen #PA5-27436), Cy3-conjugated mouse anti-GFAP (1:500, Sigma #C9205) for

24 h at room temperature. Slices were then washed in PBS-Tx and incubated in AlexaFluor647 goat anti-mouse (1:500, Invitrogen #A32733) for 2 h at room temperature. Both primary and secondary antibody incubations were done in PBS-Tx (+ 2% NGS). Slices were then washed in PBS-Tx, then PBS, prior to mounting coverslips with VectaShield + DAPI (Vector Labs #H-1200-10). Images were captured on an Olympus VS110 Slide Scanner**.** Area of Iba1 and GFAP reactivity were evaluated by setting an intensity threshold where hippocampal intensity was zero in sham, the area of positive pixels in the ipsilesional hemisphere was then determined. For GCaMP6f expression, the hippocampus was outlined based on anatomical structure in the DAPI channel, the percentage of pixels that were GCaMP6f-positive were then determined.

Analysis & Statistics

The scripts (v0.0.2) used to process and analyse fiber photometry and behavioral data are available at https://doi.org/10.5281/zenodo.8303055. GraphPad Prism 9.0 software was used for statistical analyses. Statistical tests for each experiment are described in the figure legends (data presented as mean ± s.e.m.).

Data availability

Data available upon reasonable request.

Acknowledgments

We thank Cheryl Breiteneder and Rodney Barasi for technical assistance and Núria Daviu Abant and Adam Institoris for careful review of the manuscript. We thank the Cumming School of Medicine Optogenetics Platform for fiber photometry training. We thank SciDraw for use of open-source drawings. This research was funded by operating grants to R.J.T. from the Canadian Institute for Health Research (PJT 169174 & PJT 168968) and the Krembil Foundation and to G.C.T. from a Natural Sciences & Engineering Research Council of Canada (NSERC) Discovery Grant (RGPIN/04140-2019). AKJB was supported by an Alberta Innovates (2+1) postdoctoral fellowship and a Donald Burns & Louise Berlin Postdoctoral Fellowship in Dementia Research.

Author Contributions

AKJB & RJT designed the study. AKJB performed all *in vivo* stroke & behavior recordings, analyzed data, prepared figures, and wrote/edited the manuscript. YF & CMS performed immunohistochemistry. RG performed electrode implants and assisted with LFP recording. LM wrote photometry and DLC analysis scripts. TF created behavior state analysis macro. CE analyzed some behavioral data. WN wrote behavioral state analysis script. RJT & GCT supervised the study.

Declaration of Interest

No conflicts of interest.

References

1. Campbell, B. C. V. *et al.* Ischaemic stroke. *Nat. Rev. Dis. Prim.* **5**, (2019).
2. Ali, M. *et al.* Sex Differences in Presentation of Stroke: A Systematic Review and Meta-Analysis. *Stroke* **53**, 345–354 (2022).
3. Reeves, M. J., Fonarow, G. C., Zhao, X., Smith, E. E. & Schwamm, L. H. Quality of care in women with ischemic stroke in the GWTG program. *Stroke* **40**, 1127–1133 (2009).
4. Boehme, A. K. *et al.* Sex differences in rt-PA utilization at hospitals treating stroke: The National Inpatient Sample. *Front. Neurol.* **8**, 6–11 (2017).
5. Lorenzano, S. *et al.* Does sex influence the response to intravenous thrombolysis in ischemic stroke?: Answers from safe implementation of treatments in stroke-international stroke thrombolysis register. *Stroke* **44**, 3401–3406 (2013).
6. Dreier, J. P. & Reiffurth, C. The Stroke-Migraine Depolarization Continuum. *Neuron* **86**, 902–922 (2015).
7. Leao, A. A. P. Spreading Depression of Activity in the Cerebral Cortex. *J. Neurophysiol.* **7**, 359–390 (1944).
8. Kraio, R. P. & Nicholson, C. Extracellular ionic variations during spreading depression. *Neuroscience* **3**, 1045–1059 (1978).
9. Enger, R. *et al.* Dynamics of ionic shifts in cortical spreading depression. *Cereb. Cortex* **25**, 4469–4476 (2015).
10. Binder, N. F. *et al.* Vascular Response to Spreading Depolarization Predicts Stroke Outcome. *Stroke* **53**, 1386–1395 (2022).
11. von Bornstädt, D. *et al.* Supply-demand mismatch transients in susceptible peri-infarct hot zones explain the origins of spreading injury depolarizations. *Neuron* **85**, 1117–1131 (2015).
12. Andrew, R. D. *et al.* The Critical Role of Spreading Depolarizations in Early Brain Injury: Consensus and Contention. *Neurocrit. Care* **37**, 83–101 (2022).
13. Sugimoto, K. *et al.* Optogenetic Spreading Depolarizations Do Not Worsen Acute Ischemic Stroke Outcome. *Stroke* **54**, 1110–1119 (2023).
14. Shuttleworth, C. W. *et al.* Which Spreading Depolarizations Are Deleterious To Brain Tissue? *Neurocrit. Care* **32**, 317–322 (2020).
15. Otori, T., Greenberg, J. H. & Welsh, F. A. Cortical spreading depression causes a long-lasting decrease in cerebral blood flow and induces tolerance to permanent focal ischemia in rat brain. *J. Cereb. Blood Flow Metab.* **23**, 43–50 (2003).
16. Yanamoto, H. *et al.* Induced spreading depression activates persistent neurogenesis in the subventricular zone, generating cells with markers for divided and early committed neurons in the caudate putamen and cortex. *Stroke* **36**,

1544–1550 (2005).
17. Urbach, A., Baum, E., Braun, F. & Witte, O. W. Cortical spreading depolarization increases adult neurogenesis, and alters behavior and hippocampus-dependent memory in mice. *J. Cereb. Blood Flow Metab.* **37**, 1776–1790 (2017).
18. Dell'Orco, M. *et al.* Repetitive Spreading Depolarization induces the activation of cell differentiation, synaptic plasticity, and neuroprotective pathways. *bioRxiv* (2023).
19. Urbach, A., Redecker, C. & Witte, O. W. Induction of neurogenesis in the adult dentate gyrus by cortical spreading depression. *Stroke* **39**, 3064–3072 (2008).
20. Witte, O. W., Bidmon, H. J., Schiene, K., Redecker, C. & Hagemann, G. Functional differentiation of multiple perilesional zones after focal cerebral ischemia. *J. Cereb. Blood Flow Metab.* **20**, 1149–1165 (2000).
21. Urbach, A., Brueckner, J. & Witte, O. W. Cortical spreading depolarization stimulates gliogenesis in the rat entorhinal cortex. *J. Cereb. Blood Flow Metab.* **35**, 576–582 (2015).
22. Rosenblum, W. I. & El Sabban, F. Platelet aggregation in the cerebral microcirculation. Effect of aspirin and other agents. *Circ. Res.* **40**, 320–328 (1977).
23. Watson, B. D., Dietrich, W. D., Busto, R., Wachtel, M. S. & Ginsberg, M. D. Induction of reproducible brain infarction by photochemically initiated thrombosis. *Ann. Neurol.* **17**, 497–504 (1985).
24. Chen, T.-W. *et al.* Ultrasensitive fluorescent proteins for imaging neuronal activity. *Nature* **499**, 295–300 (2013).
25. Fluri, F., Schuhmann, M. K. & Kleinschnitz, C. Animal models of ischemic stroke and their application in clinical research. *Drug Des. Devel. Ther.* **9**, 3445–3454 (2015).
26. Seto, A. *et al.* Induction of ischemic stroke in awake freely moving mice reveals that isoflurane anesthesia can mask the benefits of a neuroprotection therapy. *Front. Neuroenergetics* **6**, 1–9 (2014).
27. Balbi, M. *et al.* Targeted ischemic stroke induction and mesoscopic imaging assessment of blood flow and ischemic depolarization in awake mice. *Neurophotonics* **4**, 1 (2017).
28. Jia, J. M. *et al.* Control of cerebral ischemia with magnetic nanoparticles. *Nat. Methods* **14**, 160–166 (2017).
29. Choi, D. W. Excitotoxicity: Still Hammering the Ischemic Brain in 2020. *Front. Neurosci.* **14**, (2020).
30. Mathis, A. *et al.* DeepLabCut: markerless pose estimation of user-defined body parts with deep learning. *Nat. Neurosci.* **21**, 1281–1289 (2018).
31. Hartings, J. A. *et al.* The continuum of spreading depolarizations in acute cortical lesion development: Examining Leão's legacy. *J. Cereb. Blood Flow Metab.* **37**,

1571–1594 (2017).
32. Herreras, O., Largo, C., Ibarz, J. M., Somjen, G. G. & Del Río, R. M. Role of neuronal synchronizing mechanisms in the propagation of spreading depression in the in vivo hippocampus. *J. Neurosci.* **14**, 7087–7098 (1994).
33. Kim, J. J. & Fanselow, M. S. Modality-specific retrograde amnesia of fear. *Science (80-.).* **256**, 675–677 (1992).
34. Phillips, R. G. & LeDoux, J. E. Differential Contribution of Amygdala and Hippocampus to Cued and Contextual Fear Conditioning. *Behavioral Neuroscience* vol. 106 274–285 (1992).
35. Tovote, P., Fadok, J. P. & Lüthi, A. Neuronal circuits for fear and anxiety. *Nat. Rev. Neurosci.* **16**, 317–331 (2015).
36. O'Collins, V. E. *et al.* 1,026 Experimental treatments in acute stroke. *Ann. Neurol.* **59**, 467–477 (2006).
37. Balbi, M. *et al.* Gamma frequency activation of inhibitory neurons in the acute phase after stroke attenuates vascular and behavioral dysfunction. *Cell Rep.* **34**, 108696 (2021).
38. Silasi, G., She, J., Boyd, J. D., Xue, S. & Murphy, T. H. A mouse model of small-vessel disease that produces brain-wide-identified microocclusions and regionally selective neuronal injury. *J. Cereb. Blood Flow Metab.* **35**, 734–738 (2015).
39. Song, H. *et al.* Capsular stroke modeling based on somatotopic mapping of motor fibers. *J. Cereb. Blood Flow Metab.* **37**, 2928–2937 (2017).
40. Kuroiwa, T. *et al.* Development of a rat model of photothrombotic ischemia and infarction within the caudoputamen. *Stroke* **40**, 248–253 (2009).
41. Blanco-Suárez, E. Photothrombotic Model to Create an Infarct in the Hippocampus. *Methods Mol. Biol.* **2616**, 29–38 (2023).
42. Kumral, E. & Zirek, O. Major neurocognitive disorder followıng isolated hippocampal ischemıc lesions. *J. Neurol. Sci.* **372**, 496–500 (2017).
43. Ruan, J. & Yao, Y. Behavioral tests in rodent models of stroke. *Brain Hemorrhages* **1**, 171–184 (2020).
44. Thompson, S. M., Berkowitz, L. E. & Clark, B. J. Behavioral and neural subsystems of rodent exploration. *Learn. Motiv.* **61**, 3–15 (2018).
45. Böhm, M. *et al.* Neurovascular coupling during optogenetic functional activation: Local and remote stimulus-response characteristics, and uncoupling by spreading depression. *J. Cereb. Blood Flow Metab.* **40**, 808–822 (2020).
46. Aiba, I. & Noebels, J. L. Kcnq2/Kv7.2 controls the threshold and bi-hemispheric symmetry of cortical spreading depolarization. *Brain* **144**, 2863–2878 (2021).
47. Devaux, J. J., Kleopa, K. A., Cooper, E. C. & Scherer, S. S. KCNQ2 Is a Nodal K+ Channel. *J. Neurosci.* **24**, 1236–1244 (2004).
48. Lorincz, A. & Nusser, Z. Cell-type-dependent molecular composition of the axon initial segment. *J. Neurosci.* **28**, 14329–14340 (2008).

49. Kudo, C., Harriott, A. M., Moskowitz, M. A., Waeber, C. & Ayata, C. Estrogen modulation of cortical spreading depression. *J. Headache Pain* **24**, 1–12 (2023).
50. Houben, T. *et al.* Optogenetic induction of cortical spreading depression in anesthetized and freely behaving mice. *J. Cereb. Blood Flow Metab.* **37**, 1641–1655 (2017).
51. Bender, F. *et al.* Theta oscillations regulate the speed of locomotion via a hippocampus to lateral septum pathway. *Nat. Commun.* **6**, (2015).
52. Chen, Y. T. *et al.* Inhibitory hippocampus-medial septum projection controls locomotion and exploratory behavior. *Front. Synaptic Neurosci.* **15**, (2023).
53. Eichenbaum, H. The role of the hippocampus in navigation is memory. *J. Neurophysiol.* **117**, 1785–1796 (2017).
54. Kempermann, G., Song, H. & Gage, F. H. Neurogenesis in the Adult Hippocampus. *Cold Spring Harb. Perspect. Biol.* **7**, a018812 (2015).
55. Füzesi, T., Daviu, N., Wamsteeker Cusulin, J. I., Bonin, R. P. & Bains, J. S. Hypothalamic CRH neurons orchestrate complex behaviors after stress. *Nat. Commun.* **7**, 1–14 (2016).